29. Pietrzyk U, Herholz K, Fink K, et al. An interactive technique for three-dimensional image registration: validation for PET, SPECT, MRI and CT brain studies. *J Nucl Med* 1994;35:2011–2018.
30. Podreka I, Asenbaum S, Brücke T, et al. Intraindividual reproducibility of HMPAO brain uptake [Abstract]. *J Cereb Blood Flow Metab* 1991;11(suppl 1):S776.
31. Bonte FJ, Stokely EM, Devous MD, Homan RW. Single-photon tomographic determination of regional cerebral blood flow in epilepsy. *Am J Neuroradiol* 1983;3: 544–546.
32. Duncan R, Patterson J, Hadley DM, Wyper DJ, McGeorge AP, Bone I. Technetium-99m HMPAO single photon emission CT in temporal lobe epilepsy. *Acta Neurol Scand* 1990;81:287–293.
33. Marks D, Chou A, Katz A, Hoffer P, Spencer S. SPECT in patients with CNS heterotopias [Abstract]. *Epilepsia* 1990;31:669.
34. Henkes H, Hosten N, Cordes M, Neumann K, Hansen ML. Increased rCBF in gray matter heterotopias detected by SPECT using ^{99m}Tc hexamethyl-propylenamine oxime. *Neuroradiology* 1991:310–312.
35. Leiderman DB, Balish M, Sato S, Kufta C, Reeves P, Theodore WH. Comparison of PET measurements of cerebral blood flow and glucose metabolism for the localization of human epileptic foci. *Epilepsy Res* 1992;13:153–158.
36. Elger CE, Lehnertz K. Ictogenesis and chaos. In: Wolf P, ed. *Epileptic seizures and syndromes*. London: John Libbey and Company Ltd.; 1994:541–546.
37. Lehnertz K, Elger CE. Spatio-temporal dynamics of the primary epileptogenic area in temporal lobe epilepsy characterized by neuronal complexity loss. *Electroencephalogr Clin Neurophysiol* 1995;95:108–117.

In Vitro and In Vivo Primate Evaluation of Carbon-11-Etomidate and Carbon-11-Metomidate as Potential Tracers for PET Imaging of the Adrenal Cortex and Its Tumors

Mats Bergström, Thomas A. Bonasera, Li Lu, Elisabeth Bergström, Carin Backlin, Claes Juhlin and Bengt Långström
Subfemtomole Biorecognition Project, Japan Sciences Technology Corporation and Uppsala University PET Centre, and Department of Surgery, University Hospital, Uppsala, Sweden

Methods: With the purpose of developing a PET imaging agent for tumors of the adrenal cortex, we developed syntheses for ^{11}C-etomidate and its methyl analog, ^{11}C-metomidate. (R)-[O-ethyl-1-^{11}C]Etomidate and (R)-[O-methyl-^{11}C]metomidate were prepared by reaction of the appropriate respective ^{11}C-labeled alkyl iodide and the tetrabutylammonium salt of the carboxylic acid derivative. The specificity of binding to the adrenal cortex was tested through the use of frozen section autoradiography of different tissues of the rat, pig and human. Inhibition of tracer binding was evaluated with etomidate, ketoconazole and metyrapone, well-known inhibitors of enzymes for steroid synthesis. Tracer binding to different human tumor samples was compared to immunohistochemical staining with antibodies for the steroid synthesis enzymes P450 11β (11β-hydroxylase), P450 scc (cholesterol side-chain cleavage enzyme), P450 C21 (21-hydroxylase) and P450 17α (17α-hydroxylase). Three PET investigations, one with ^{11}C-etomidate and two with ^{11}C-metomidate, were performed in rhesus monkey sections, including the adrenals, liver and kidneys. Time-activity curves were generated from measured tracer uptake in these organs. **Results:** In frozen section autoradiography of various tissues, high binding was seen in the adrenal cortex from all species, as well as in the tumors of adrenal cortical origin. The level of liver binding was about 50% of that in the adrenals, whereas that of all other organs was <10% of the adrenal binding. The adrenal binding was blocked by etomidate and ketoconazole at low doses but not by metyrapone. The binding in the adrenal tumor samples correlated with immunostaining for P450 11β. PET studies in the monkey demonstrated high uptake in the adrenals with excellent visualization. The uptake increased with time without indication of washout. Slightly lower uptake was seen in the liver as compared to the adrenals, and in the late images, no organs other than adrenals and liver were seen. **Conclusion:** These investigations indicate that ^{11}C-etomidate and ^{11}C-metomidate have the potential to be useful specific agents for the visualization of the normal adrenal cortex and to provide positive identification of adrenal cortical tumors.

Received Jun. 18, 1997; revision accepted Sep. 27, 1997.
For correspondence or reprints contact: Mats Bergström, PhD, Uppsala University PET Centre, University Hospital, S-751 85 Uppsala, Sweden.

Key Words: PET; adrenal cortex; steroid synthesis; etomidate; 11β-hydroxylase
J Nucl Med 1998; 39:982–989

As a result of the increased use of CT, MRI and ultrasound, incidentally found masses in the location of the adrenal glands have emerged as a clinical problem. Patients undergoing CT for reasons other than suspected adrenal disease manifest adrenal lesions with a frequency of approximately 1% (*1–3*). The potential extent of this problem is illustrated by the fact that adrenal lesions are found at autopsy in 1.9%–8.7% (*4,5*). In most cases (70%–94%), these incidentally found tumors, termed "incidentalomas," consist of benign cortical nonhypersecretory adenomas (*6*). If an adrenal lesion has been radiologically detected in a patient, a biochemical hormonal screening is performed to rule out both adrenal medullary and cortical hypersecretory tumors. If hypersecretion is established biochemically, these patients are normally considered candidates for surgery. For patients without evidence of adrenal hypersecretion, the differentiation of the common adenomas from other benign lesions such as cysts and lipomas or from malignant lesions, i.e., adrenal cortical carcinoma or extra-adrenal metastasis, must be established. In view of the low specificity of CT, MRI and other imaging methods for such differentiation, patients with nonhypersecretory tumors that are >3 cm in diameter are often referred for surgery to rule out a primary adrenal cortical carcinoma.

Iodine-123-iodomethylnorcholesterol (NP-59) imaging (*7–9*) has a high specificity and accuracy in defining adrenal cortical masses. A limitation of the method is the long waiting period (4–7 days) from injection to imaging, making it cumbersome and costly. Both hypersecretory and nonhypersecretory adenomas (and some hypersecretory adrenal cortical carcinomas) accumulate NP-59, whereas nonfunctioning primary and secondary malignant lesions, as well as other space-occupying lesions, demonstrate decreased, distorted or absent uptake.

Using NP-59 scintigraphy in 229 patients, Gross et al. (*10*) demonstrated 100% specificity and 70% sensitivity in characterizing clinically silent adrenal masses found by CT. In their report, however, only 15% of the NP-59 avid lesions (adrenal adenomas) were confirmed by surgery. Boland et al. (*11*) used PET with ^{18}F-fluorodeoxyglucose to show an excellent discrimination between benign adrenal lesions with no uptake and adrenal metastases characterized by high uptake. The development of adrenal cortical imaging agents based on enzyme inhibitors was reported by Beierwaltes et al. (*12,13*). The ^{11}C radiolabeling of an analog of metyrapone, a potent and selective inhibitor of 11β-hydroxylase activity, has been reported (*14*), but these researchers concluded from results of rat biodistribution studies, that this tracer was not a viable candidate for the in vivo PET imaging of 11β-hydroxylase activity in humans. "Faint adrenal images" were reported when ^{123}I-metyrapone was used in one patient with bilateral hyperplasia (*15*). Thus, successful human studies of enzyme inhibitor-based adrenal cortical imaging have not been reported.

To more efficiently discriminate adrenal cortical masses from nonadrenal masses presenting as incidentalomas on CT and to visualize and lateralize small hyperfunctioning adrenal adenomas that are not clearly depicted by CT, we hypothesized that PET might be potentially valuable, with its vast potential for using radiolabeled substances.

As a biochemical target, we selected the cortisol- and aldosterone-synthesizing enzymes, which should be found exclusively in lesions originating from the adrenal cortex. As the potentially best tracer substance, we chose etomidate, which has been shown to be the most potent available inhibitor of 11β-hydroxylase (*16–19*), a key enzyme in the biosynthesis of cortisol and aldosterone. Etomidate, first reported in the 1960s and 1970s and manufactured by Janssen Pharmaceutica, is an imidazole derivative with short-acting hypnotic properties when it is administered intravenously and has, thus, been used as an anesthetic in humans (*20*). Incubation studies with human adrenocortical tissue have shown that etomidate predominantly blocks the conversions of 11-deoxycortisol to cortisol (IC_{50} = 0.15 μM) and of 11-deoxycorticosterone to corticosterone (IC_{50} = 0.03 μM) (*16,17*) by inhibition of the cytochrome P450-linked 11β-hydroxylase enzyme system. Etomidate also inhibits 17α-hydroxylase (IC_{50} = 6–8 μM) and, much less potently, the production of androstendione from 17α-hydroxyprogesterone (IC_{50} = 380 μM). Etomidate has no inhibitory effect on 21-hydroxylase.

During the development of the labeling methods for ^{11}C-etomidate, we also investigated the methylated form, ^{11}C-metomidate. Both of these compounds were tested in vitro using frozen section autoradiography and in vivo in biodistribution studies in the rhesus monkey to explore their potential as tracers for the adrenal cortex and its tumors.

MATERIALS AND METHODS

Chemistry

Synthesis of Carbon-11-Labeled Ethyl Iodide. Carbon-11-CO_2 was produced on a Scanditronix MC-17 cyclotron. After cryogenic focusing, ^{11}C-CO_2 was transferred in a stream of nitrogen to a glass reaction vessel that had been charged with MeMgBr (36 μmol, 0.3 ml of a 0.12 *M* solution diluted 1:24 in Et_2O-tetrahydrofuran; Aldrich) 30 sec after the cryogenic ^{11}C-CO_2 trap was removed from its liquid nitrogen bath. After the amount of radioactivity that passed through the reaction vessel and trapped in an Ascarite tube had peaked (~2.5 min), $LiAlH_4$ (0.2 mmol, 0.2 ml of a 1 *M* solution in tetrahydrofuran; Aldrich) was added. The nitrogen flow was increased to 200 ml/min, and the vessel was heated to 130°C over 3 min. The nitrogen flow was reduced to 10 ml/min. A second reaction vessel connected in series to the first was charged with HI (0.5 ml, 57%; Fluka), and the same amount of HI was added to the first reaction vessel over 30 sec. After an additional 30 sec, the second reaction vessel was heated to 130°C over 3 min, and the volatile components were distilled through a Sicapent drying column into the substrate vial over 7 min.

Preparation of the Precursor. (*R*)-1-(1-Phenylethyl)-1*H*-imidazole-5-carboxylic acid (R28141, 22.8 mg, 105 μmol; Cilag-Janssen Pharmaceutica) was weighed into a 5-ml glass vial. Water (2 ml) and methylene chloride (2 ml) were added, followed by tetra-n-butylammonium hydroxide (60 μl of a 1.5 *M* aqueous solution, 90 μmol; Aldrich). The vial was equipped with a magnetic stirring bar and capped, and the solution was stirred for 18 hr at room temperature. The organic phase was removed, passed through a $MgSO_4$ plug and filtered into a flask. Solvent was removed in vacuo and the residue was dissolved in 2.2 ml DMF(N,N-dimethylformamide) (Aldrich). Each of eight oven-dried 0.8-ml glass high-performance liquid chromatography (HPLC) vials was charged with 250 ml of the resulting solution. The vials were crimp-capped and stored below 0°C before use.

Synthesis of [O-Ethyl-1-Carbon-11]Etomidate. Carbon-11-ethyl iodide was distilled into the precursor solution in the HPLC vial described above. The vial was heated in a 130°C aluminum block for 7 min. The vial contents were purified by HPLC (Beckman Ultrasphere ODS, 5 mm, 10 × 250 mm, 45% ethanol/55% water, 5 ml/min, 254-nm mass detection, radioactivity detection), and [O-ethyl-1-^{11}C]etomidate (ETO) was collected from ~9.9–11.8 min. For in vitro experiments, the tracer was diluted directly from the HPLC eluent. For in vivo PET experiments, the mobile phase was removed in vacuo at 120°C, and the residue was dissolved in 10% ethanol/90% phosphate buffer (pH 7.4). The product was analyzed by analytical HPLC for the concentration of etomidate and for radiochemical purity [Beckman Ultrasphere ODS, 5 mm, 4.6 × 250 mm, 65% acetonitrile:methanol (1:1)/35% water, 1 ml/min, 254-nm mass detection, radioactivity detection, t_R (etomidate standard) = 7.7 min].

Synthesis of [O-Methyl-Carbon-11]Metomidate. Carbon-11-methyl iodide (prepared from [^{11}C]CO_2, $LiAlH_4$ and HI) was distilled into the precursor vial, proceeding as described above for ETO. [*O-Methyl*-^{11}C]metomidate (MTO) was collected from the preparative HPLC column from ~6.5–7.8 min. For in vivo experiments, the product was formulated directly by diluting a 1-ml aliquot of HPLC eluent with 8 ml of phosphate buffer. The product was analyzed by analytical HPLC for the concentration of metomidate and for radiochemical purity [Beckman Ultrasphere ODS, 5 mm, 4.6 × 250 mm, 60% acetonitrile:water (50:7)/40% 50 m*M* ammonium formate (pH 3.5), 1 ml/min, 254-nm mass detection, radioactivity detection, t_R (metomidate standard) = 5.2–5.3 min].

Frozen-Section Autoradiography

Various tissues from rats and pigs (adrenal gland, liver, lung, heart, kidney, bladder, colon, rectum, prostate, pancreas and brain), complemented with human tissues (normal adrenal gland, adrenal tumors, pancreatic cancer, uterine leiomyoma and synovia from rheumatoid arthritis), were rapidly frozen and stored at −70°C. Frozen sections with a thickness of 25 μm were cut with a cryostat microtome, adhered to gelatinized glass slides, well-dried at +4°C and stored at −20°C awaiting the experiments. For the binding studies, the glass-mounted tissues were preincubated for 10 min in

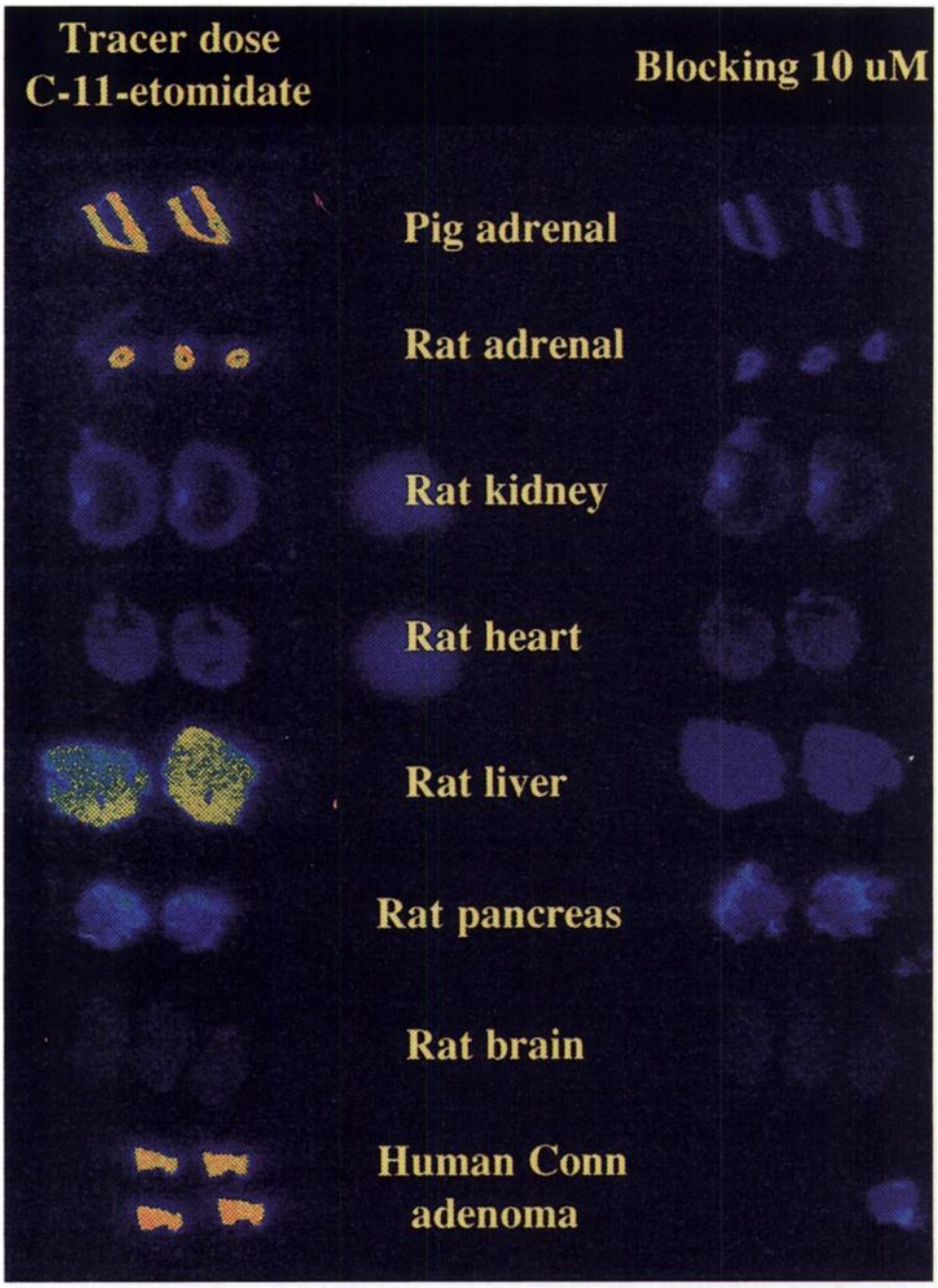

FIGURE 1. Frozen-section autoradiography performed by incubating tissue slices with ^{11}C-etomidate at a 30 n*M* concentration for 30 min, washing and exposing on phosphor imaging plate. Parallel samples were coincubated with 10 μM etomidate to indicate nonspecific binding.

Tris-HCl buffer (pH 7.4). Carbon-11-etomidate or ^{11}C-metomidate was added at a concentration of 30 n*M*, and incubation proceeded for 30 min at room temperature. Parallel sections were incubated with radioactivity plus 10 μM of etomidate for blocking specific binding. Thereafter, the sections were washed three times for 1 min on each occasion in buffer and then once in purified water and finally dried for 10 min at +37°C. A reference incubation standard was prepared by placing 20 μl of the incubation solution on a small filter paper attached to a glass slide. The mounted sections were placed on a storage phosphor screen (PhosphorImager; Molecular Dynamics) for an exposure of 40 min (*21,22*). The plate was read by a laser, and a quantitative image of the distribution of radioactivity was viewed on a computer screen. For quantification of binding, regions of interest (ROIs) were outlined on the sections, the incubation standard, the blocked sections and a background area of the screen. After subtraction of the background, specific binding in a tissue section was calculated as total binding minus uptake in a blocked section of the corresponding tissue, and the fraction of specific binding was calculated as the ratio of specific binding to total binding. The specific binding was further corrected for variations in specific radioactivity by dividing by the total measured radioactivity in the incubation standard.

In separate experiments, the influence of incubation time was investigated by incubation of pig adrenal and pig liver sections for 10, 20, 30, 40 and 50 min. The influence of washing time was investigated by incubating for 30 min and washing three times for 1 min each time, and thereafter, the sections were left in the last washing bath for another 10, 20, 30 or 40 min. The inhibition of ^{11}C-metomidate binding to pig adrenal and liver sections was examined either by adding nonradioactive etomidate at concentrations up to 10 μM together with the radioactivity or by adding etomidate at concentrations up to 3.3 μM 60 min before the radioactivity was added. Similar blocking studies at similar concentrations were performed with ketoconazole and metyrapone.

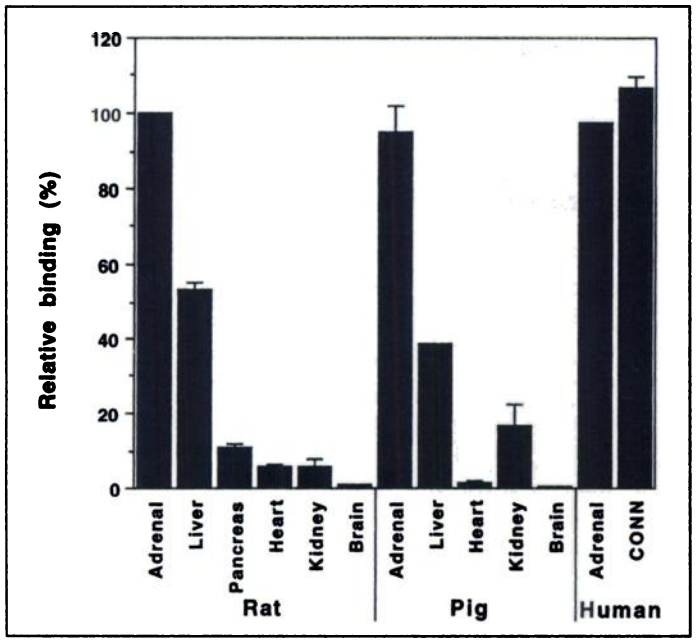

FIGURE 2. Relative specific binding of ^{11}C-etomidate to frozen sections from rat, pig and human tissues. Normalized to rat adrenal cortex binding (100%). Bars, s.d.

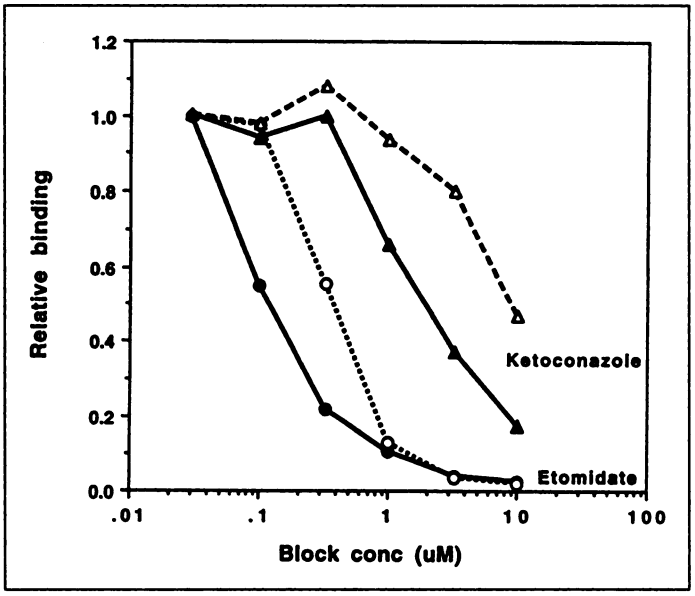

FIGURE 4. Semilogarithmic plot of inhibition of ^{11}C-metomidate binding to pig adrenal cortex exerted by etomidate (○ and ●) and ketoconazole (△ and ▲) at increasing doses. The inhibitor was added either 60 min before (● and ▲) or simultaneously with tracer (○ and △).

Adrenal Tissues and Immunhistochemistry

One biopsy from a normal adrenal gland was obtained during nephrectomy and biopsies from 13 adrenocortical tumors during adrenal surgery. The adrenal tumors consisted of six adenomas (1–4 cm in diameter) and seven adrenal cortical carcinomas (7–15 cm in diameter). Of the adenomas, two were associated with primary hyperaldosteronism (Conn's syndrome), two were associated with hypersecretion of cortisol and two were associated with nonfunctioning status. Of the carcinomas, one was associated with hypersecretion of estradiol, one was associated with hypersecretion of estradiol, cortisol and androgens and the remaining five were associated with no biochemical evidence of hormone excess. All patients with carcinomas demonstrated a pathological urine steroid profile with increased urinary excretion of mainly 3β-hydroxy-5-ene steroids and tetrahydro-11-deoxycortisol (*23*).

The immunohistochemical staining was performed on 6-μm acetone-fixed cryosections. As primary antisera, rabbit polyclonal antibodies generated against the following enzymes were used: bovine cytochrome P450 11β-hydroxylase (P450 11β, diluted 1:50; Oxygene Dallas, Dallas, TX) (*24*), porcine 17α-hydroxylase (P450 17α, diluted 1:70; Oxygene Dallas) (*25*) and bovine side-chain cleavage enzyme (P450 scc, diluted 1:30; Oxygene Dallas) (*26*). In addition, human antisera containing autoantibodies to cytochrome P450 21-hydroxylase were used (P450 C21, diluted 1:150) (*27*). The sections were then incubated with biotinylated goat antirabbit IgG (BA1000, diluted 1:200; Vector Laboratories, Burlinghame, CA) or peroxidase-labeled rabbit antihuman IgG (P214, diluted 1:200; DAKO, Glostrup, Denmark), followed by incubation of avidin–biotin–horseradish peroxidase complex (PK4000; Vector). As negative control normal rabbit IgG (Z0113;

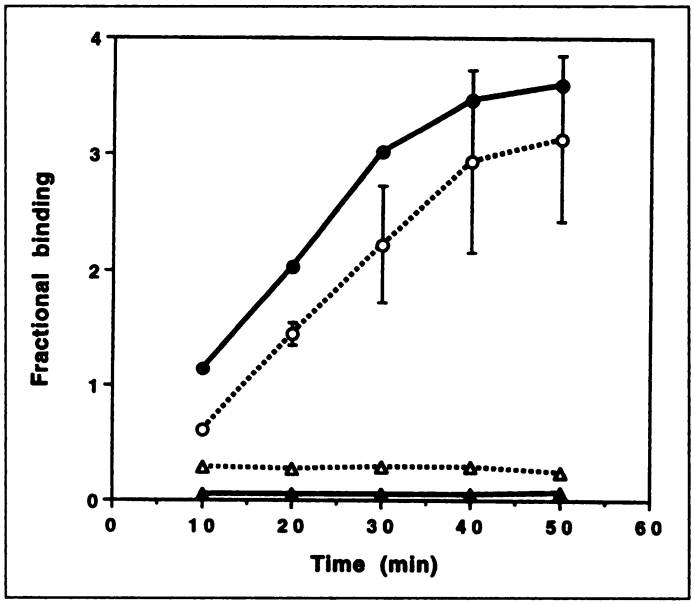

FIGURE 3. Time course of binding of ^{11}C-etomidate (○ and △) and ^{11}C-metomidate (● and ▲) to pig adrenal slices. Lower lines (△ and ▲) indicate amount of nonspecific binding.

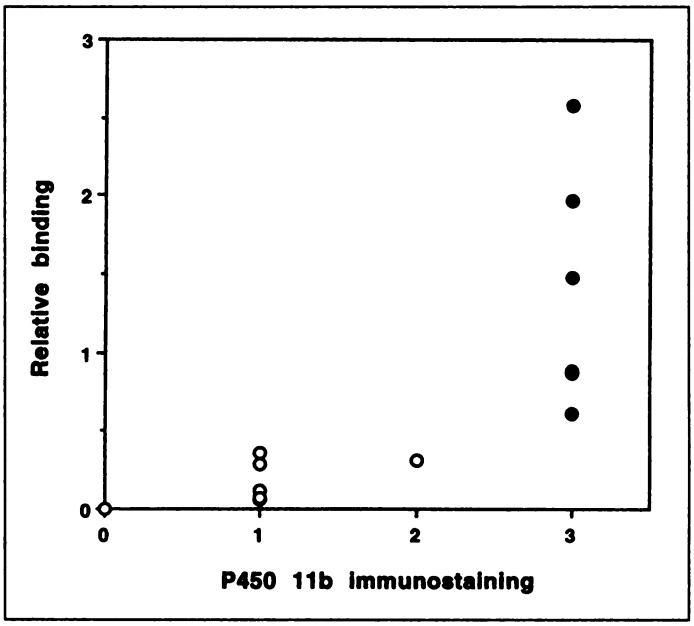

FIGURE 5. Relative binding of ^{11}C-metomidate to 13 operative samples of adrenal tumors correlated with the degree of immunostaining (scale, 0 = no staining to 3 = strong staining) for 11β-hydroxylase. ○ = cancers; ● = adenomas.

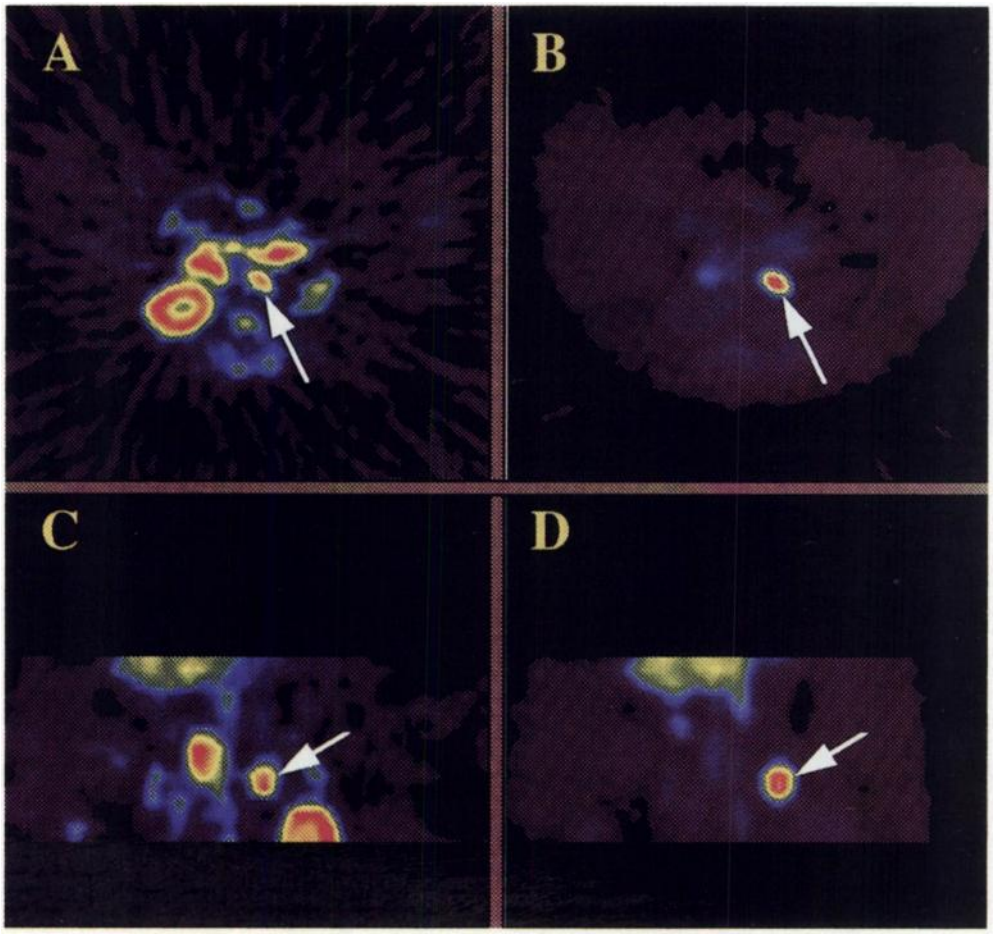

FIGURE 6. PET images obtained after intravenous injection of ^{11}C-metomidate in rhesus monkeys. Left images (A and C) show the uptake pattern 0.5 min after injection, and right images (B and D) corresponding sections 20 min after injection. Upper images (A and B) show axial sections, and lower images (C and D) show parasagittal sections through the right kidney and adrenal. Arrow indicates adrenal cortex.

DAKO) and normal human serum obtained from a blood donor were used in the same concentrations as the primary antisera. Staining was visualized by 3-amino-9-ethylcarbazole (KEBO Laboratories, Spånga, Sweden) and counterstained with Mayer's hematoxylin. All antisera were diluted in phosphate-buffered saline containing 1% bovine serum albumin (Sigma Chemical Co., St. Louis, MO), and all incubations were performed at room temperature.

Immunoreactivity, reported as semiquantitative staining intensity, was classified as follows: 0 = none, 1 = weak, 2 = moderate and 3 = strong.

Monkey Studies

Three rhesus monkeys were selected for PET investigations. The monkeys were anesthetized with diprivan and tracrium and prepared for artificial ventilation. The monkeys were placed supine on the bed of the PET camera (GE 4096) (*28*) and positioned to allow the 10-cm field of view to image the abdomen including the adrenals. A transmission scan was performed using an external ^{68}Ge source. Carbon-11 etomidate (one study) or ^{11}C-metomidate (two studies) (95–135 MBq) was injected intravenously and scanning was initiated with a dynamic imaging sequence in which 14 frames were acquired over 45 min. Quantitative images were reconstructed with attenuation and scatter correction. In the images obtained, ROIs were manually outlined to represent adrenals, liver, kidney and pancreas. Well-perfused organs, such as the kidneys and the pancreas, were identified in early images. For each region and each study, time-activity data were generated, expressed as the standardized uptake value (SUV) by dividing the regional tracer concentration by the ratio of total administered radioactivity to body weight. Time-activity data were plotted to allow a comparison of behavior of the two tracers in the selected organs. To further demonstrate the selective tracer uptake in the adrenals as compared to liver, the ratios of adrenal to liver were formed and plotted versus time.

RESULTS

Radiochemistry

Syntheses of ETO and MTO were prepared by reaction of the appropriate respective ^{11}C-labeled alkyl iodide and the tetrabutylammonium salt of the carboxylic acid derivative. Up to 1.6 GBq of ETO with a specific radioactivity of up to 6.4 GBq/μmol was prepared in less than 60 min from the end of cyclotron bombardment, whereas up to 10 GBq of MTO with a specific radioactivity of up to 120 GBq/μmol was prepared in under 40 min.

Autoradiography

The images from frozen-section autoradiography performed with ^{11}C-etomidate demonstrated high binding in adrenals from all species including man, as well as in the Conn's adenoma (Fig. 1). Relatively high binding was also noted in the livers, whereas other organs had low binding. Quantitatively, the binding in the adrenals from rats, pigs and humans differed by less than 10% (Fig. 2). Liver binding was 40%–50% of adrenal binding, kidney binding was 6%–16% and binding of all other organs was $<$10%.

When binding studies were performed with ^{11}C-metomidate in different tissues, the highest uptake was noted in the adrenals from the rat and pig (^{11}C-metomidate was not studied in human adrenals), followed by livers from these two species. Liver binding was about 26% of the respective adrenal binding.

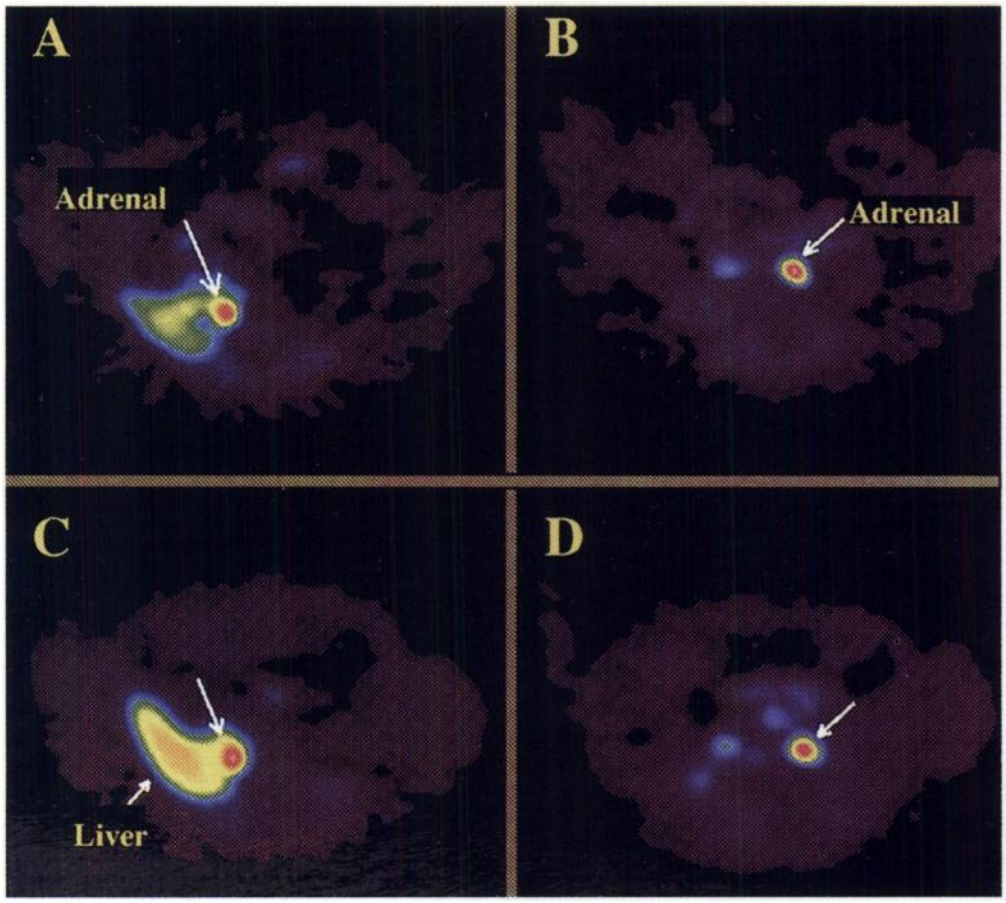

FIGURE 7. Axial images of the monkey abdomen at the levels of the right adrenal (A and C) and left adrenal (B and D). Upper images (A and B) were obtained with the injection of ^{11}C-etomidate, and lower images (C and D) were obtained with ^{11}C-metomidate.

Binding to rat pancreas was 4%, and binding to rat and pig kidney was about 1%. All other tissues, including human pancreas cancers, uterine leiomyoma and inflammatory synovia, had binding of <1% of that seen in the adrenals.

There was a good correlation between the binding of ^{11}C-etomidate and ^{11}C-metomidate ($R^2 = 0.95$), but in general, the binding to the adrenals was higher for ^{11}C-metomidate and the binding to other organs was lower for this tracer.

Incubation with ^{11}C-etomidate or ^{11}C-metomidate for different lengths of time resulted in a nearly linear increase in the bound fraction (Fig. 3). With the longest incubation time (50 min), a tendency for equilibration was seen. After a 30-min incubation time, the nonspecific binding was 13% for ^{11}C-etomidate and 2% for ^{11}C-metomidate. A 30-min incubation, followed by washing for different time periods, indicated no loss of radioactivity for either of the tracers.

In the competition experiments, the specific binding of ^{11}C-metomidate to pig adrenal sections was inhibited in a dose-dependent manner by etomidate with an IC_{50} of 0.4 μM if the blocking agent was added simultaneously with the tracer and with an IC_{50} of 0.13 μM if it was added 60 min before (Fig. 4). In studies of the ^{11}C-etomidate and ^{11}C-metomidate binding to liver slices, the specific binding was much lower than in the adrenals. This binding was inhibited at lower etomidate concentrations, 0.09 and 0.07 μM, respectively. Ketoconazole inhibited the ^{11}C-metomidate binding to adrenal sections with an IC_{50} of 9.5 μM when it was given simultaneously with tracer and with an IC_{50} of 2.3 μM when it was given 60 min before. In the liver sections, the inhibition constants were 6.1 and 2.1 μM, respectively. When attempts were made to inhibit ^{11}C-metomidate binding with metyrapone, no effect was seen up to 10 μM.

Immunohistochemistry revealed significant differences between the different tissue samples studied. No correlation could be found between the degree of ^{11}C-metomidate binding and the immunohistochemical staining for P450 17α. Compared to immunohistochemistry for P450 scc and P450 C21, the ^{11}C-metomidate binding was, on average, higher in those sections with intense staining, but there was a wide range from close to zero to the highest values. There was a clear overlap in ^{11}C-metomidate binding between sections with weak staining and those with strong staining.

With respect to staining for P450 11β, there was a clear correlation to ^{11}C-metomidate binding with high binding in those sections showing strong staining and low binding in those with weak staining (Fig. 5). There was no overlap in binding between those with strong staining compared to the others. There was also a clear separation of adenomas and cancers, with the adenomas all having strong staining and high binding of ^{11}C-metomidate (mean ± s.d., 1.40 ± 0.76) and the cancers showing faint or weak staining and low binding (0.17 ± 0.15).

Monkey Studies

In the PET images acquired immediately after injection, high uptake was noted in the kidney cortex and pancreas (Fig. 6). After only a few minutes, the adrenals exhibited the highest uptake of those tissues in the field of view of the PET camera. At the end of the study, only the adrenals and the liver could be seen, with significantly higher uptake in the adrenals. Visually, no clear difference was noted between ^{11}C-metomidate and ^{11}C-etomidate (Fig. 7). The time course of uptake in the kidney and pancreas was characterized by very high initial values (SUV ~15), followed by a marked washout (SUV ~2–3) (Fig. 8). The adrenal uptake increased rapidly within the first few minutes, followed by a slower increase to SUV levels of 15–20. The liver showed a tendency to reach a plateau (ETO) or slow

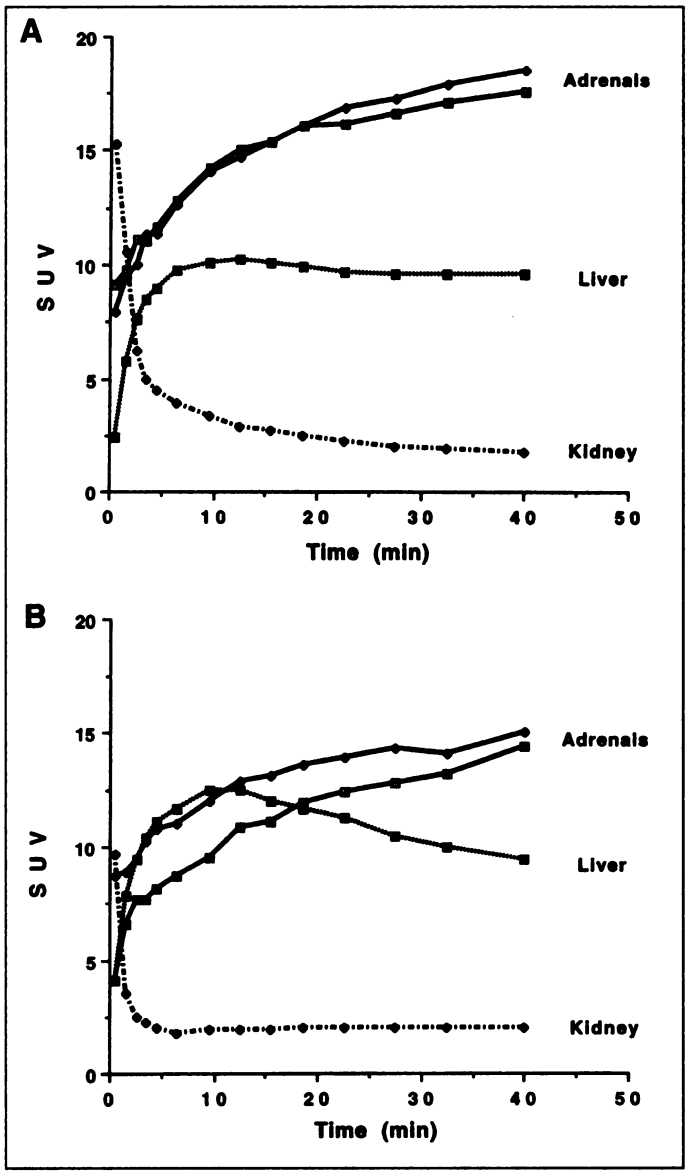

FIGURE 8. Time-activity curves of adrenals, liver and kidney, expressed in SUV, in PET studies in monkeys performed with ^{11}C-etomidate (A) and ^{11}C-metomidate (B).

decrease (MTO) after a maximum at about 10 min after injection. The final liver SUV level achieved was about 10 for both tracers.

The adrenal-to-liver ratio showed a minimum at about 5 min after injection, followed by almost linear increases with time to reach ratios of 1.3 for ^{11}C-metomidate and 1.8 for ^{11}C-etomidate.

DISCUSSION

While searching the literature for suitable agents that could be used for the identification of adrenal cortex tumors, it was logical to focus on one specific property of the adrenal cortex, namely, the biosynthesis of the steroids cortisol and aldosterone. This synthesis proceeded from cholesterol through several hydroxylation and other cytochrome P450 enzymes. We assumed that tracers with specific binding to any of these enzymes should have a high specificity for binding to the adrenal cortex and lesions originating from there. Etomidate, an ethyl carboxylic acid ester, has been reported to be the most potent inhibitor of the adrenal steroid synthesis system known (*19*) and, hence, was a logical choice for the attempt to find a suitable PET tracer. Metomidate, the methyl ester derivative of etomidate, has similar inhibitory properties. Each inhibitor could be readily synthesized in ^{11}C-labeled form in amounts suitable for in vivo and in vitro studies, although both the radiochemical yields and specific radioactivities were significantly higher for MTO than ETO. The lower yields and specific activities obtained in the synthesis of ETO can be directly attributed to the nonoptimized synthesis of [^{11}C]ethyl iodide. The method provided a mixture of ^{11}C iodides (methyl, ethyl and isopropyl) (*29*), and the presence of ethyl iodide mass could likely be caused by a combination of the high reactivity of methyl magnesium bromide with atmospheric carbon dioxide and hydrolysis of residual diethyl ether in the reaction medium.

Frozen-section autoradiography performed with ETO and MTO demonstrated that the binding of these tracers was high in normal adrenal cortex tissues without any major interspecies differences. The binding was basically irreversible in the time span available for ^{11}C-labeled compounds. As an indication that the binding observed is likely to be related to binding to 11β-hydroxylase, this binding is blocked by etomidate and ketoconazole at doses correlating well with 11β-hydroxylase inhibition constants (*16–19*). Finally, there was a good correlation between the binding of ^{11}C-metomidate and staining with an antibody to 11β-hydroxylase. However, one factor that remains to be explained is the lack of competition by metyrapone, a well-known inhibitor of 11β-hydroxylase. The reason for this discrepancy may be that ETO and MTO bind preferentially to one isoenzyme while metyrapone binds to another or that the compounds bind to different sites on the enzyme.

The monkey studies demonstrate that ^{11}C-metomidate and ^{11}C-metomidate are also suitable in vivo tracers. Although the adrenal cortex in the monkey is smaller than the resolution element of the PET camera, the adrenals were clearly delineated and had higher uptake than did any other structure in the abdomen. This points to the possibility of visualizing the adrenals and lesions derived from them in vivo in humans, and indeed, we have already shown this in a pilot study (Bergström M, *unpublished data*, 1997).

Certain disorders that manifest themselves as lesions in the adrenal cortex may have steroid-synthesizing properties similar to or quite different from those of the surrounding tissue. Benign adenoma, for example, has been shown to have increased levels of 11β-hydroxylase (*30,31*). Other lesions found in the adrenal cortex, such as adrenal cancer, may have varying levels of this and other steroid biosynthetic enzymes, as the limited number of tumors investigated implies. Lesions of nonadrenal origin, such as metastases originating from lung, breast and colorectal cancers, which frequently metastasize to the adrenal cortex, are expected to not have the mechanisms of adrenal steroid biosynthesis and, therefore, to not contain enzymes such as 11β-hydroxylase. The method presented when applied in vivo in humans, should, therefore, allow a good discrimination between lesions of adrenal cortical origin and metastases from other tumor sites or pheochromocytomas and could potentially influence therapeutic and surgical decisions in patient care.

CONCLUSION

In vitro studies using ^{11}C-etomidate and ^{11}C-metomidate have indicated high uptake in the adrenal cortex of three species, including man, and very low uptake in most other organs. In vivo imaging of the adrenals was possible in the monkey with good visualization. It is thus likely that either of these two tracers will allow in vivo imaging of the adrenal cortex and its tumors to be used for diagnostic or differential diagnostic purposes. With a shorter synthesis time and higher

radiochemical yields and specific radioactivities, ^{11}C-metomidate is more suitable for future clinical studies.

ACKNOWLEDGMENTS

This work was supported by grants from the Swedish Cancer Society, Uppsala Lions Foundation, Åke Wibergs Foundation and the Swedish Natural Sciences Research Council (Grant K3463 to Bengt Långström) and by postdoctoral fellowships from the Swedish Cancer Fund (to Thomas A. Bonasera), National Science Foundation (Grant INT-9505394 to Thomas A. Bonasera) and Fulbright Commissions of the United States and Sweden (to Thomas A. Bonasera). Etomidate, metomidate and R28141 were kindly supplied by Janssen Research Foundation (Beerse, Belgium).

REFERENCES

1. Glazer HS, Weyman PJ, Sagel SS, Levitt RG, McClennan BL. Nonfunctioning adrenal masses: incidental discovery on computed tomography. *Am J Radiol* 1982;139:89–95.
2. Mitnick JS, Bosniak MA, Megibow AJ, Naidich DP. Nonfunctioning adrenal adenomas discovered incidentally on CT. *Radiology* 1985;148:495–499.
3. Belldegrunn A, Hussain S, Seltzer SE, Louhlin KR, Gites RF, Richie JP. Incidentally discovered mass of the adrenal gland. *Surg Gynecol Obstet* 1986;163:203–208.
4. Abbecassis M, McLoughlin MJ, Langer B, Kudlow JE. Serendipitous adrenal masses: prevalence, significance and management. *Am J Surg* 1985;149:783–788.
5. Hedeland H, Östberg G, Hökfelt B. On the prevalence of adrenocortical adenomas in an autopsy material in relation to hypertension and diabetes. *Acta Med Scand* 1968;184:211–214.
6. Kloos RT, Gross MD, Francis IR, Korobkin M, Shapiro B. Incidentally discovered adrenal masses. *Endocrinol Rev* 1995;16:460–484.
7. Schteingart DE, Seabold JE, Gross MD, Swanson DP. Iodocholesterol adrenal tissue uptake and imaging in adrenal neoplasms. *J Clin Endocrinol Metab* 1981;52:1156–1161.
8. Ishimura J, Kawakanaka M, Fukuchi M. Clinical application of SPECT in adrenal imaging with iodine-131 6β-iodomethyl-19-norcholesterol. *Clin Nucl Med* 1989;14:278–281.
9. Kazerooni EA, Sisson JC, Shapiro B, et al. Diagnostic accuracy and pitfalls of (iodine-131)6-beta-iodomethyl-19-norcholesterol (NP-59) imaging. *J Nucl Med* 1990;31:526–534.
10. Gross MD, Shapiro B, Francis IR, et al. Scintigraphic evaluation of clinically silent adrenal masses. *J Nucl Med* 1994;35:1145–1152.
11. Boland GW, Goldberg MA, Lee MJ, et al. Indeterminate adrenal mass in patients with cancer: evaluation at PET with 2-(F-18)-fluoro-2-deoxy-D-glucose. *Radiology* 1995;194:131–134.
12. Beierwaltes WH, Wieland DM, Mosley ST, et al. Imaging of the adrenal glands with radiolabeled inhibitors of enzymes: concise communication. *J Nucl Med* 1978;2:200–203.
13. Beierwaltes WH, Wieland DM, Ice RD, et al. Localization of radiolabeled enzyme inhibitors in the adrenal gland. *J Nucl Med* 1976;11:998–1002.
14. Damani LA, Mitterhauser M, Zolle I, Lin G, Oehler E, Ho YP. Metabolic and pharmacokinetic considerations in the design of 2-phenyl substituted metyrapone derivatives: 2-methoxyphenylmetyrapone as a radioligand for functional diagnosis of adrenal pathology. *Nucl Med Biol* 1995;22:1067–1074.
15. Robien W, Zolle I. Synthesis of radioiodinated metyrapone: a potential adrenal imaging agent. *Int J Appl Radiat Isot* 1983;34:907–914.
16. Varga I, Rács K, Kiss R, et al. Direct inhibitory effect of etomidate on corticosteroid secretion in human pathologic adrenocortical cells. *Steroids* 1993;58:64–68.
17. Weber MM, Lang J, Abedinpour F, Zeilberger K, Adelmann B, Engelhardt D. Different inhibitory effect of etomidate and ketoconazole on the human adrenal steroid biosynthesis. *Clin Invest* 1993;71:933–938.
18. Engelhardt D, Weber MM. Therapy of Cushing's syndrome with steroid biosynthesis inhibitors. *J Steroid Biochem Mol Biol* 1994;49:261–267.
19. Engelhardt D. Steroid biosynthesis inhibitors in Cushing's syndrome. *Clin Invest* 1994;72:481–488.
20. Gooding JM, Corssen G. Etomidate: an ultrashort-acting nonbarbituate agent for anesthesia induction. *Anesth Analg* 1976;55:286–289.
21. Yanai K, Ryu JH, Watanabe T, Iwata R, Iso T. Receptor autoradiography with ^{11}C and (^{3}H)-labeled ligands visualized by imaging plates. *Neuroreport* 1992;3:961–964.
22. Göller L, Bergström M, Nilsson S, Westerberg G, Långström B. MAO-A enzyme binding in bladder cancer characterized with (^{11}C)harmine in frozen section autoradiography. *Oncol Rep* 1995;2:717–721.
23. Gröndahl S, Eriksson B, Hagenäs L, Werner S, Curstedt T. Steroid profile in urine: a useful tool in the diagnosis and follow up of adrenocortical carcinoma. *Acta Endocrinol* 1990;122:656–663.
24. Dutton DR, Reed GA, Parkinson A. Redox cycling of resorufin catalysed by rat liver microsomal NADPH-cytochrome P450 reductase. *Arch Biochem Biophys* 1989;268:605–616.
25. Lund J, Faucher DJ, Ford SP, Porter JC, Waterman MR, Mason JI. Developmental expression of bovine adrenocortical steroid hydroxylase: regulation of P-450 17alpha expression leads to episodic fetal cortisol production. *J Biol Chem* 1988;263:16195–16201.
26. Kramer RE, DuBois RN, Simpson ER, et al. Cell-free synthesis of precursor forms of mitochondrial steroid hydroxylase enzymes of the bovine adrenal cortex. *Arch Biochem Biophys* 1982;215:478–485.
27. Winqvist O, Rastad J, Tibell AK, Karlsson FA, Kämpe O. Expression of the Addisonian autoantigen in human adrenal tumors. *Autoimmunity* 1993;16:173–180.
28. Kops ER, Herzog H, Schmid A, Holte S, Feinendegen LE. Performance characteristics of an eight-ring whole body PET scanner. *J Comput Assist Tomogr* 1990;14:437–445.
29. Långström B, Antoni G, Gullberg P, et al. The synthesis of 1-^{11}C-labelled ethyl, propyl, butyl and isobutyl iodides and examples of alkylation reactions. *Appl Radiat Isot* 1986;37:1141–1145.
30. Suzuki H, Shibata H, Maruyama T, Ishimura Y, Saruta T. Significance of steroidogenic enzymes in the pathogenesis of hyper-functioning adrenal tumor. *Steroids* 1995;60:42–47.
31. Rács K, Pinet F, Marton T, Szendre B, Gláz E, Corvol P. Expression of steroidogenic enzyme messenger ribonucleic acids and corticosteroid production in aldosterone-producing and "nonfunctioning" adrenal adenomas. *J Clin Endocrinol Metab* 1993;77:677–682.